

soap bubble is shown in Fig. 4.40. This same concept can be applied to testing shallow etch patterns in optical element, like the spherical aberration compensators shown in Fig. 4.41. Different etch depths, which produce different phase shifts on transmission, display different colors in the Fizeau film under white-light illumination.

Newton's rings are a special type of Fizeau interference pattern formed by a circularly-symmetric quadratic wedge, as shown in Fig. 4.42. For example, if a flat plate and a spherical surface with radius  $R$  come in contact, thickness of the wedge is given by

$$t(x, y) \approx \frac{x^2 + y^2}{2R}, \quad (4.75)$$

when radius  $R$  is large. Lines of constant OPD form circular fringes. The value of  $|\text{OPD}|$  is minimum in the center of the pattern, so changes in source wavelength do not affect the center as much as the higher-order fringes at larger radii. In fact, white-light fringes are easily observed with Newton's Rings, as displayed in Fig. 4.42. Colored rings can be observed as radii increases. This phenomenon is not observable with Haidinger's fringes, even though they look similar, because  $|\text{OPD}|$  is maximum in the center of the Haidinger pattern.

#### 4.2.8 Twyman-Green interferometer

A Twyman-Green interferometer is sketched in Fig. 4.43. Collimated laser beam  $U(\mathbf{r}, t)$  illuminates both the flat reference mirror M1 and the test mirror M2 after beam splitter reflection and transmission, respectively. Path length from the beam splitter to the reference mirror is  $d_1$ , and path length from the beam splitter to the test mirror is  $d_2$ . Upon reflection from the test mirror, test beam phase is modified due to surface height  $\varepsilon(x_0, y_0)$ . Observation space begins as soon as the beams reflected from each mirror combine after the beam splitter. OPD is given by

$$\text{OPD}(x_0, y_0) = 2(d_1 - d_2) - 2\varepsilon(x_0, y_0). \quad (4.76)$$

With  $\phi$  as the phase difference of reflection from the two mirrors, bright fringes are observed when OPD satisfies Eq. (4.72). A Twyman-Green interferometer is called a *double-pass interferometer*, because the test beam OPD is modified by twice the surface departure  $\varepsilon(x_0, y_0)$ .<sup>5</sup> An interferogram made by using a Twyman-Green interferometer to test a spherical mirror is shown in Fig. 4.44. The OPD between fringes is one wave. One fringe deviation represents  $\frac{1}{2}$  wave of surface departure, due to the double-pass nature of this interferometer. A slight tilt between the reference and test waves produces straight-line cosine fringes in the interferogram. Deviations from straight lines indicate surface errors. Even without computer processing of the interferogram, sensitivities of

---

<sup>5</sup> Notice that the Fizeau interferometer, shown in Fig. 4.37, is also a double-pass interferometer.

$\lambda/8$  surface error are easily observed. Usually, an optical system in the observation space images the test mirror onto a camera, in order to avoid Fresnel diffraction effects associated with mirror features.

#### 4.2.9 Mach-Zehnder interferometer

The Mach-Zehnder interferometer also uses a collimated laser beam as the source. As shown in Fig. 4.45, a reference path and a test path are created by beam splitter BS1. Light in the reference path reflects off mirror M1 and then is directed by beam splitter BS2 into the observation space. Light in the test path transmits through the test object, reflects off mirror M2 and transmits through BS2 into the observation space. Of course, the beam splitters and mirrors must be high quality, in order not to add any phase disturbance that could be misinterpreted as being caused by the test object. A phase difference across the test beam is generated from refractive index variations or surface topology of the test sample. Interference between test and reference beams produce fringes in the observation space, which appear like those in Fig. 4.44.

Topography-induced optical path difference for a glass test object is illustrated in Fig. 4.46. Optical path length OPL is measured from a reference plane inside the glass to a measurement plane outside the glass.  $OPL_A$  of path A in a flat region of the glass surface is

$$OPL_A = n_{to} t_{ref} + \varepsilon_{offset} , \quad (4.77)$$

where  $n_{to}$  is the refractive index of the test object,  $t_{ref}$  is test object thickness from the reference plane to the flat surface and  $\varepsilon_{offset}$  is offset distance in air of the measurement plane from the flat region.  $OPL_B$  in the region of surface topography is

$$OPL_B = n_{to} t_{ref} + [\varepsilon_{offset} - \varepsilon(x, y)] n_{to} + \varepsilon(x, y) , \quad (4.78)$$

where  $\varepsilon(x, y)$  is surface sag to the measurement plane. OPD between paths A and B is

$$OPD = OPL_A - OPL_B = (n_{to} - 1) [\varepsilon(x, y) - \varepsilon_{offset}] . \quad (4.79)$$

The  $\varepsilon_{offset}$  term is not a function of position, so it can arbitrarily be set to zero, resulting in OPD mapped to the measurement plane of

$$OPD(x_0, y_0) = (n_{to} - 1) \varepsilon(x_0, y_0) + (d_1 - d_2) , \quad (4.80)$$

where  $(d_1 - d_2)$  is path difference between the reference and test arms with no defects as measured from BS1. Like with the Twyman-Green interferometer, the measurement plane is usually reimaged onto a camera in observation space, where it interferes with the plane-wave reference beam. Surface topography is directly mapped into fringe deviation.

If a small amount of tilt is introduced between reference and test beams, straight and equally spaced cosine fringes are observed in regions corresponding to flat areas of the test object. One fringe deviation due to surface topography corresponds to surface height

$$\varepsilon_{fringe} = \frac{\lambda}{n_{to} - 1} . \quad (4.81)$$

A primary difference between the Mach Zehnder interferometer and the Twyman-Green interferometer is that the Mach Zehnder is a *single-pass interferometer*, because fringe deviation is generated from a single path length through the defect.

Another interesting aspect of interferometers is illustrated with the Mach Zehnder. The combined reference and test beams at the second output of BS2 also form an interference pattern. That interference pattern is *complementary* (bright fringes become dark and dark fringes become bright) with respect to the first output of BS2.

Mach Zehnder interferometers are also useful for testing index variations in solids, measuring refractive index of gasses, determining properties of plasmas, and many other applications.

#### 4.2.10 Michelson interferometer

The basic Michelson interferometer is shown in Fig. 4.47. An extended source is used to illuminate a two-beam interferometer through beam splitter BS. At first, the Michelson interferometer is analyzed using a quasimonochromatic extended source, with endpoints  $a$  and  $b$ . After the basic concepts of fringe localization are explained, the analysis is extended to polychromatic extended sources.

The first beam of the interferometer is defined by the light reflected off BS and mirror M1, which then transmits back through BS toward the observation plane. The total path for the first beam is  $d_1 + d_3 + d_3 + d_4$ . The second beam of the interferometer is defined by the light that passes through BS, reflects off mirror M2 and then reflects off BS toward the observation plane. The total path for the second beam is  $d_1 + d_2 + d_2 + d_4$ . An imaging system is used to look into the beam splitter and form images of the fringes on an observation plane.

An unfolded diagram of the interferometer is shown in Fig. 4.48. The source images are formed by reflections off the mirrors. The images  $a_1b_1$  and  $a_2b_2$  are as far behind the mirrors as the source is in front. As shown, the mirrors are parallel to the source, so the source images are also parallel to the source and each other. From the perspective of the observer, as shown in Fig. 4.49, the source images are exactly analogous to the geometry shown in Figs. 4.33, where an extended source is used with a PPP. In this case, a simple optical system in observation space can be used to observe Haidinger's fringes at its back focus plane, as shown in Fig. 4.34 for the PPP. Separation of the coherent pairs increases as the distance  $2|d_3 - d_2|$  between source images increases, and more fringes are observed in the concentric pattern. Like with the plane parallel plate, maximum OPD is found in

the center of the pattern. The Michelson interferometer can be configured so that the two mirrors are tilted, but not displaced, as shown in Fig. 4.50. The thin space between the mirrors in the unfolded system is analogous to a Fizeau thin film. The source images are also tilted.

For small mirror tilts, an analysis similar to the one described for Fig. 4.36 shows that the  $m = 0$  fringes intersect at the mirrors, where the fringes are localized. If the mirrors are perfectly flat, straight and equally spaced fringes of equal thickness are observed when the mirrors are reimaged to the observation plane. As the tilt angle decreases, separations of the coherent pairs decrease, and fringe spacing increases. Fizeau-type fringes are observed if the mirrors are not flat, where the fringe deviation from a straight line is proportional to the surface feature.

For the case of tilted mirrors with no displacement, as shown in Fig. 4.50, the  $m = 0$  fringe intersects the mirrors. Therefore, if the source is polychromatic, good visibility can be observed until  $OPD \sim c/\Delta\nu$ , where  $\Delta\nu$  is the bandwidth of the source power spectrum. For example, if a white-light (400 nm to 700 nm) extended source is used,  $\Delta\nu \sim 2.9 \times 10^{14}$  Hz, and  $OPD \sim 10^{-6}$  m = 1  $\mu$ m before fringe visibility fades. Since the average wavelength is 550 nm, about two fringes ( $m = \pm 2$ ) can be observed with good visibility on each side of the  $m = 0$  fringe for a total of five fringes. These fringes are often called *white-light fringes*. Fringe shift due to the colored spectrum reduces fringe visibility for higher OPD, as shown in Fig. 4.51.

If the two mirrors are tilted and displaced, as shown in Fig. 4.52, the center of the localization surface is now offset from the mirrors. If the offset is not large, high visibility fringes can be observed at the mirrors. Fringes intersecting the mirrors are of high order  $m$  and some curvature due to the hyperbolic shape is observed.

A practical consequence of the beam splitter in the Michelson interferometer is that one of the beams must pass through some thickness of glass, as shown in Fig. 4.53. Light from the source first transmits through the glass of BS and then reflects off its back side toward M1. Then, it passes through the glass twice more before reaching the observation plane. On the other hand, light from the source that transmits through BS and reflects off M2 only passes through the glass once. If the optical glass used to construct BS exhibits significant dispersion, OPD contains additional wavelength-dependent terms that drastically reduce visibility when the interferometer is used with polychromatic sources. In order to balance OPD and remove effects of the dispersion, a compensator plate C is placed in the second beam of the interferometer before M2. The extra glass is fabricated from the same glass as BS, and it is the same thickness. With the compensator, the two beams pass through the same type and thickness of glass before reaching the observation plane. A student version of the Michelson interferometer is shown in Fig. 4.54 with a compensator plate.

A summary of fringe localization effects with a Michelson interferometer is shown pictorially in Fig. 4.55, where path difference increases outwardly from the center. The top row displays the case where mirrors M1 and M2 are parallel to a quasimonochromatic

extended source, which forms Haidinger's fringes. As the path difference increases, fringes expand outwardly from the center. Note that Haidinger's fringes are not observable with a white-light source. The bottom row displays the case where the mirrors are tilted and displaced. With no displacement, fringes of equal thickness are observed. If the  $m = 0$  fringe can be imaged onto the observation plane, white-light fringes can be produced. As the path difference increases with increasing displacement, the center of the fringe localization surface offsets from the mirrors, and curved fringes are observed. Larger mirror displacements offset the center of the localization surface so much that fringes are no longer observable.

#### 4.2.11 Lateral shearing interferometer (LSI)

#### 4.2.12 Radial shearing interferometer (RSI)

#### 4.2.13 Polarization splitters

#### 4.2.14 Diffraction gratings

### 4.3 Multiple-Beam Interference

#### 4.3.1 Airy's formula

#### 4.3.2 Absorbing coatings

#### 4.3.3 Fabret Perot (plane and spherical)

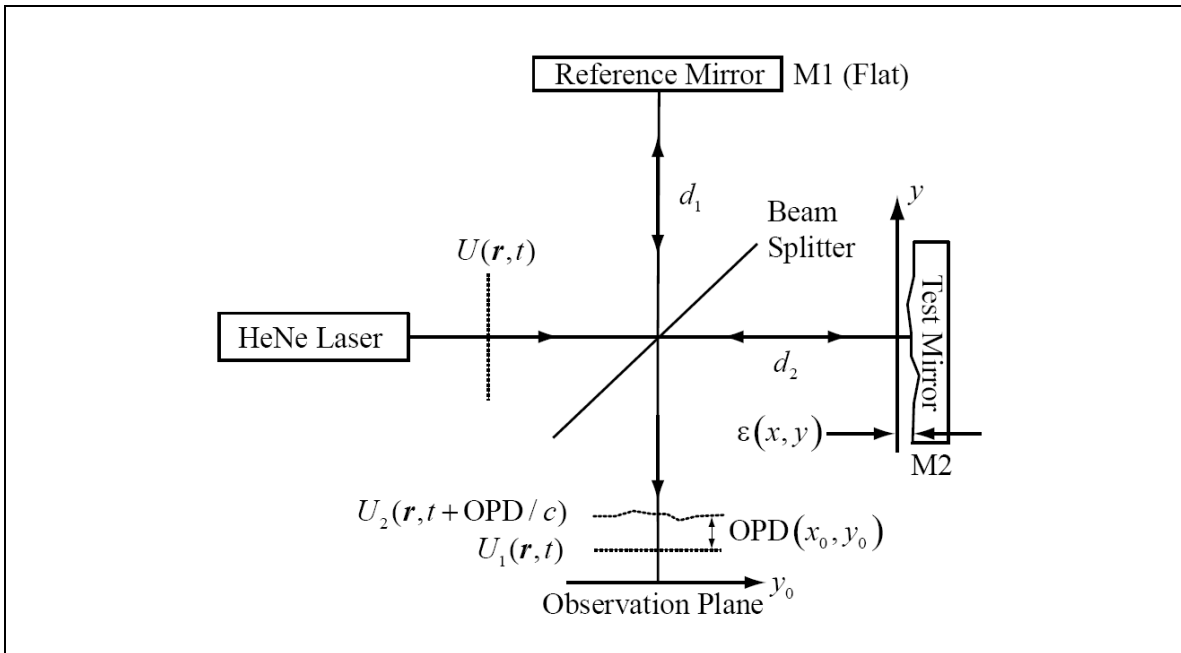


Figure 4.43. Twyman-Green Interferometer. A collimated laser beam reflects from test and reference mirrors to form the interference pattern. OPD generated from defects on the test mirror surface determines brightness of the fringe pattern.

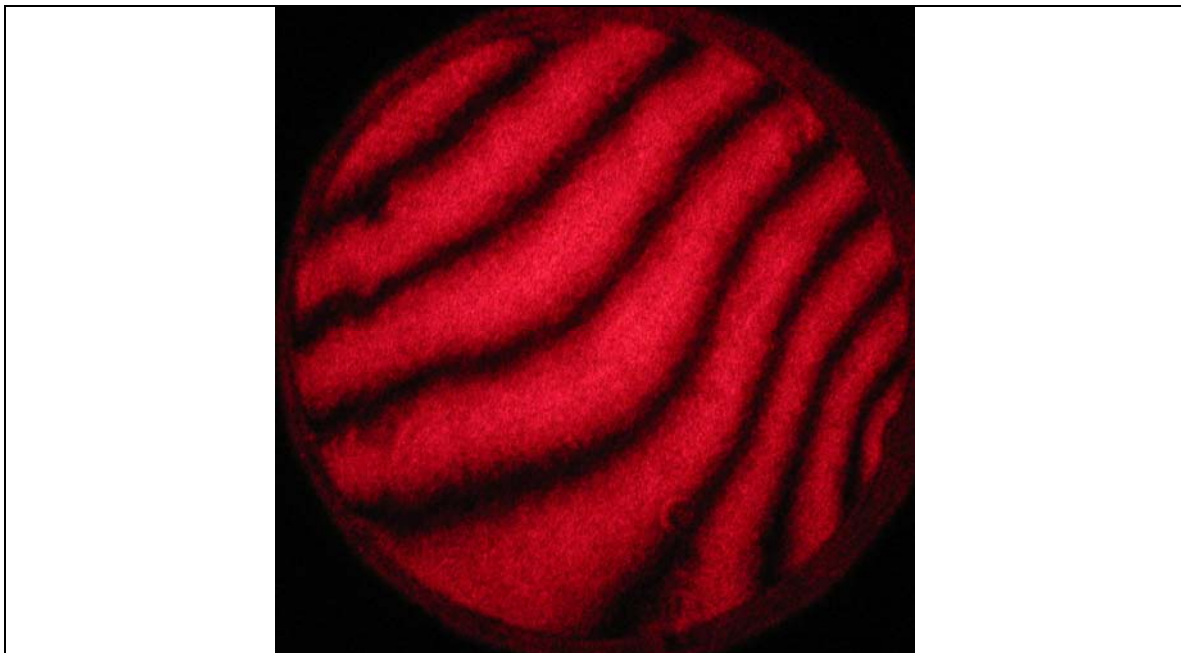


Figure 4.44. Twyman-Green test of a spherical mirror.

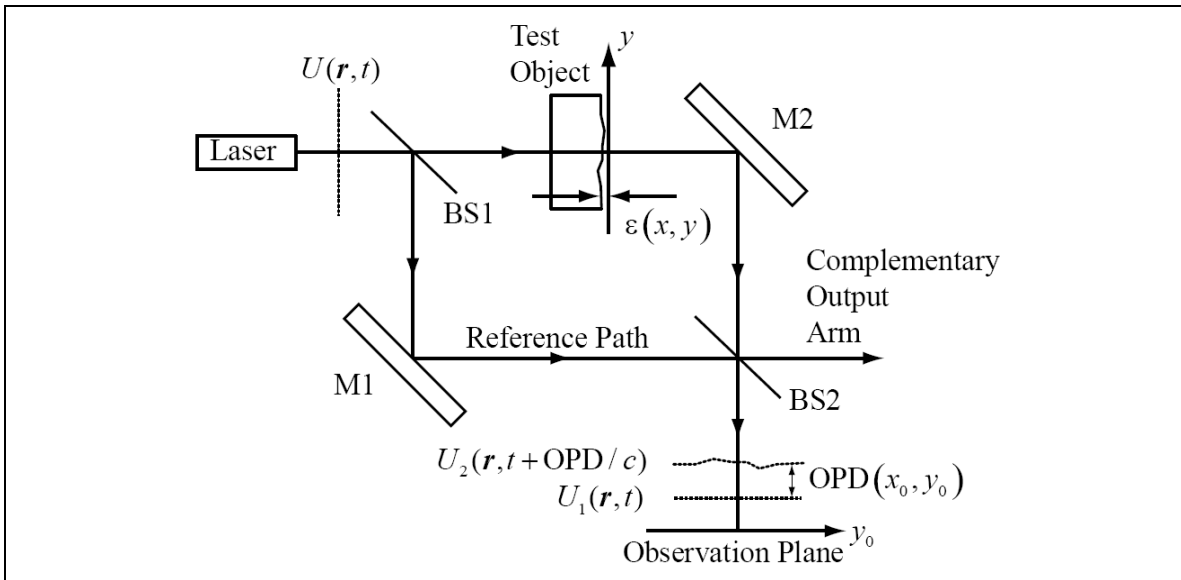


Figure 4.45. Mach Zehnder interferometer.

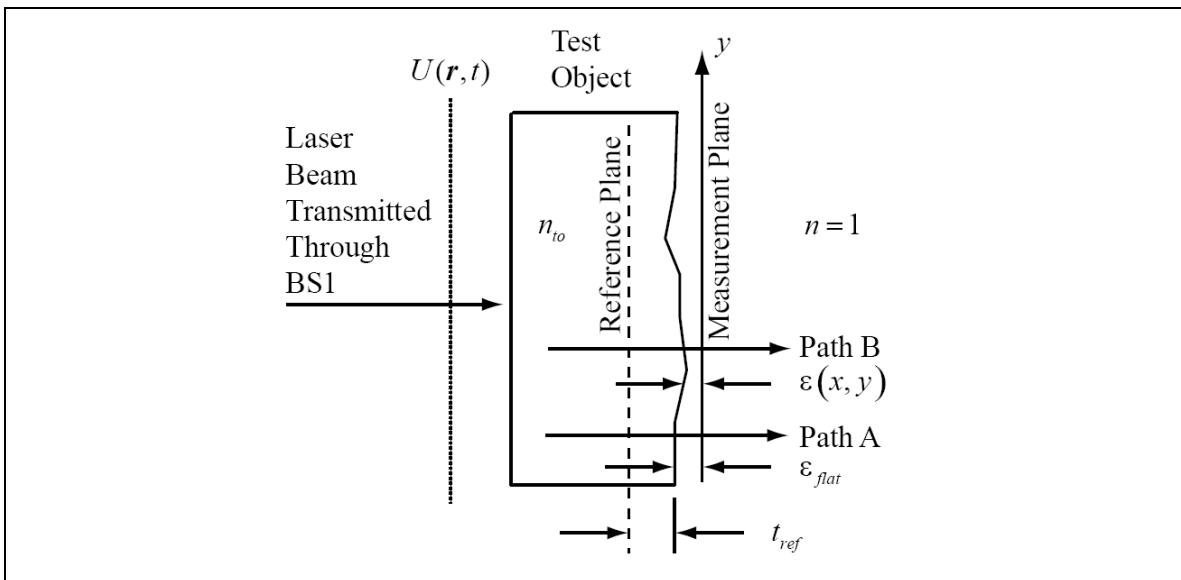


Figure 4.46. Topology-induced phase difference in transmission.

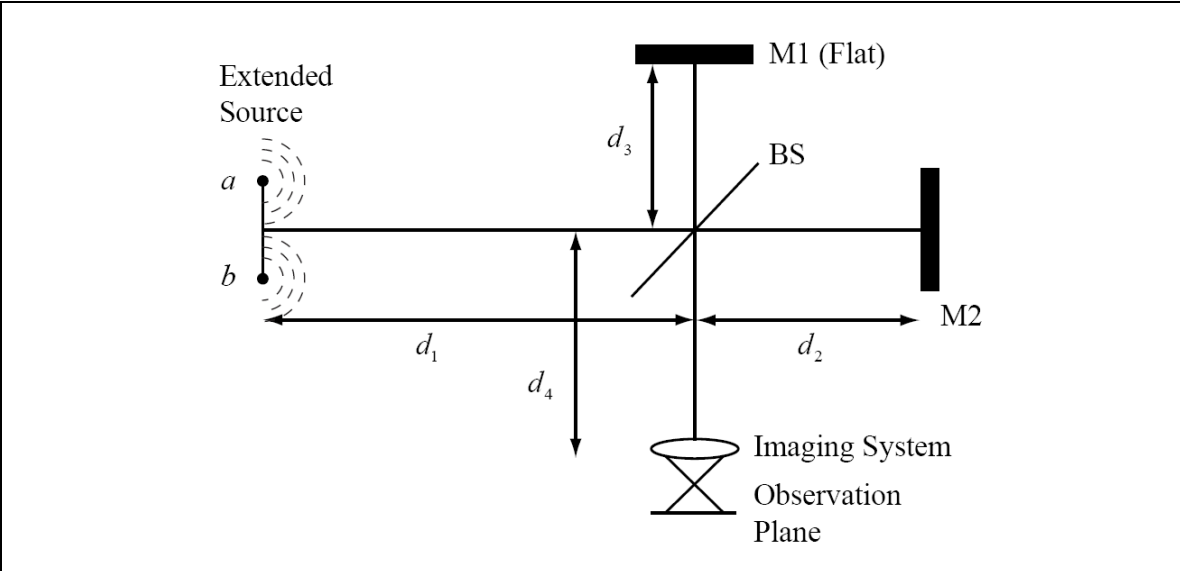


Figure 4.47. Basic Michelson interferometer.

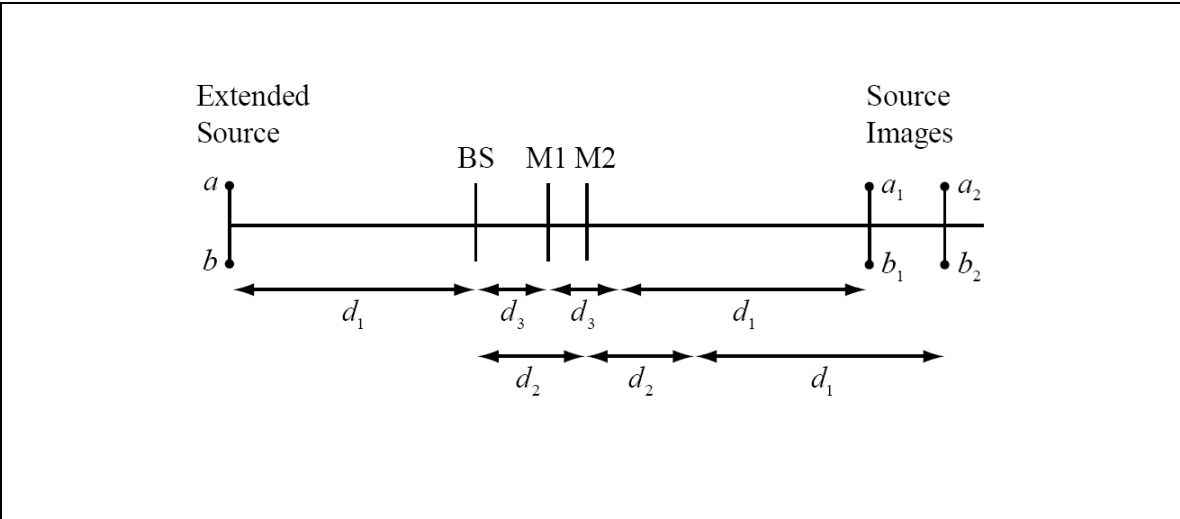


Figure 4.48. Unfolded Michelson interferometer.

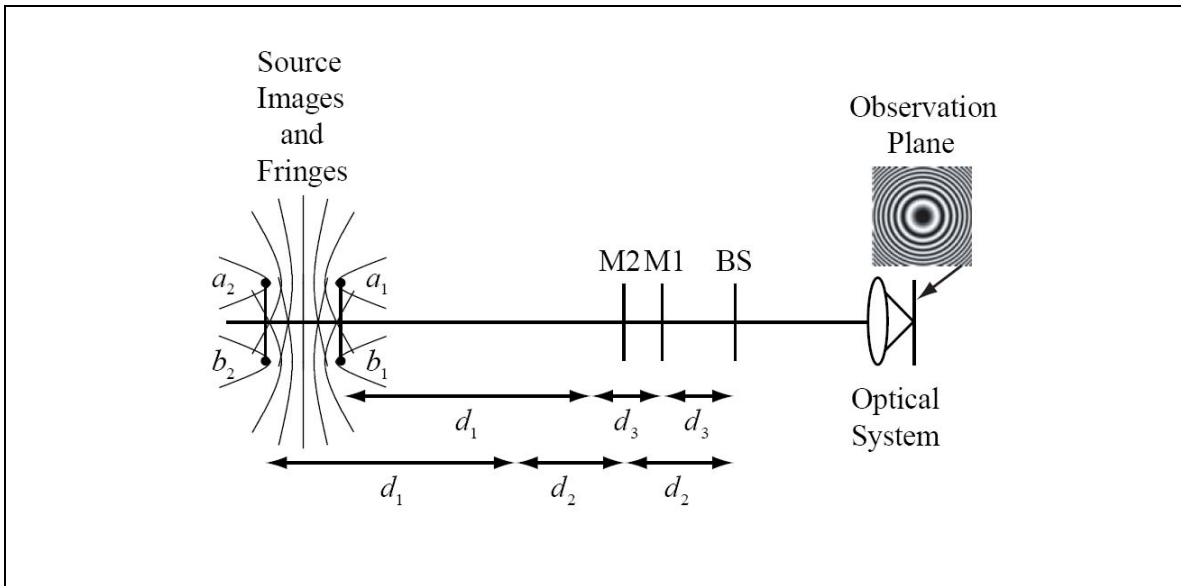


Figure 4.49. Michelson interferometer with parallel mirrors from the observer's perspective. Haidinger fringes are observed in the back focal plane of the optical system.

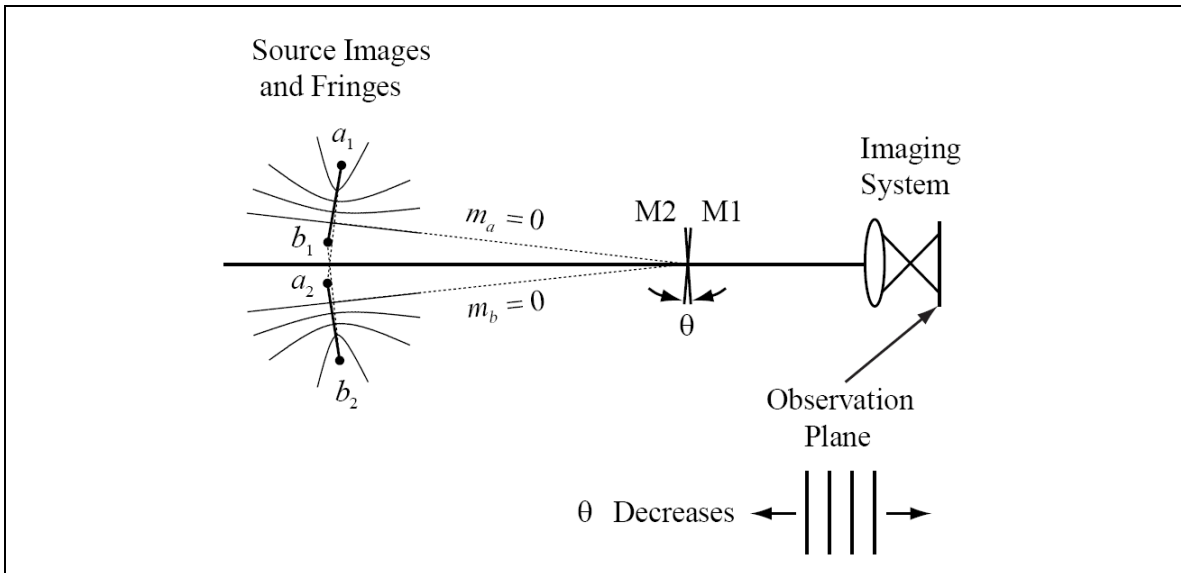


Figure 4.50. Michelson interferometer with tilted but not displaced mirrors. Fringes of equal thickness are observed when the mirrors are imaged onto the observation plane.

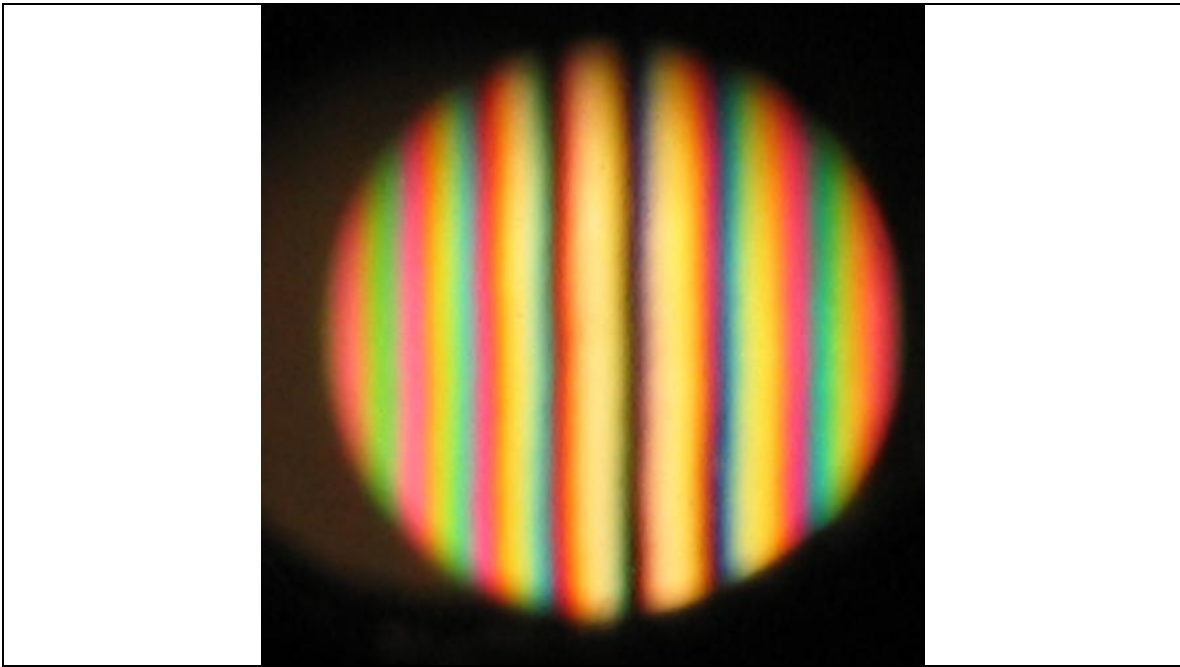


Figure 4.51. Michelson interferometer white-light fringes.

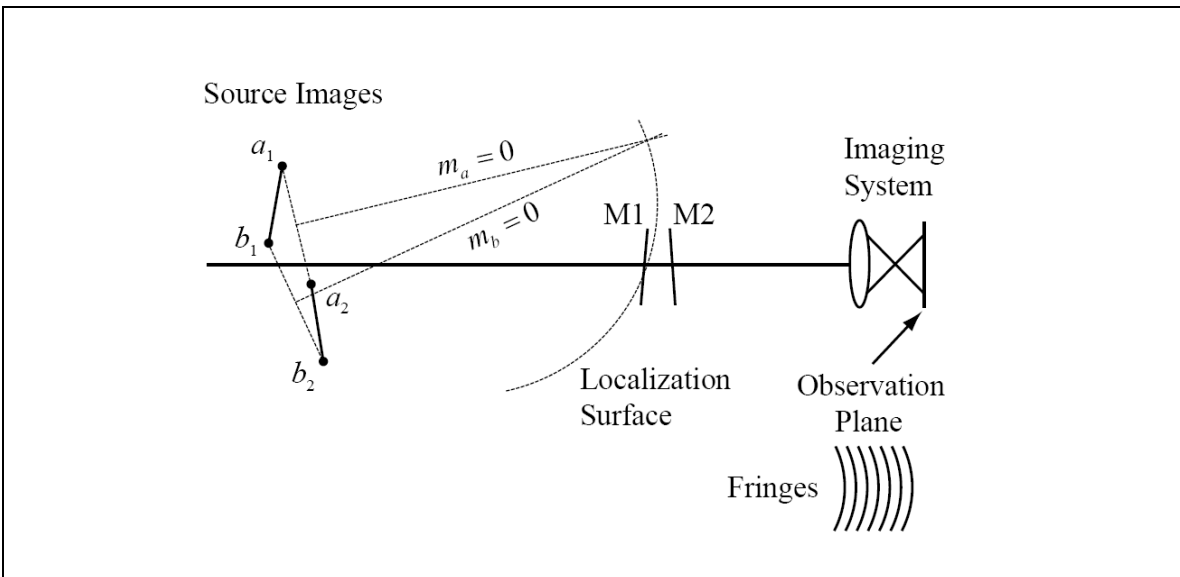


Figure 4.52. Michelson interferometer with tilted and displaced mirrors. Fringes with hyperbolic curves are observed when the mirrors are imaged onto the observation plane.

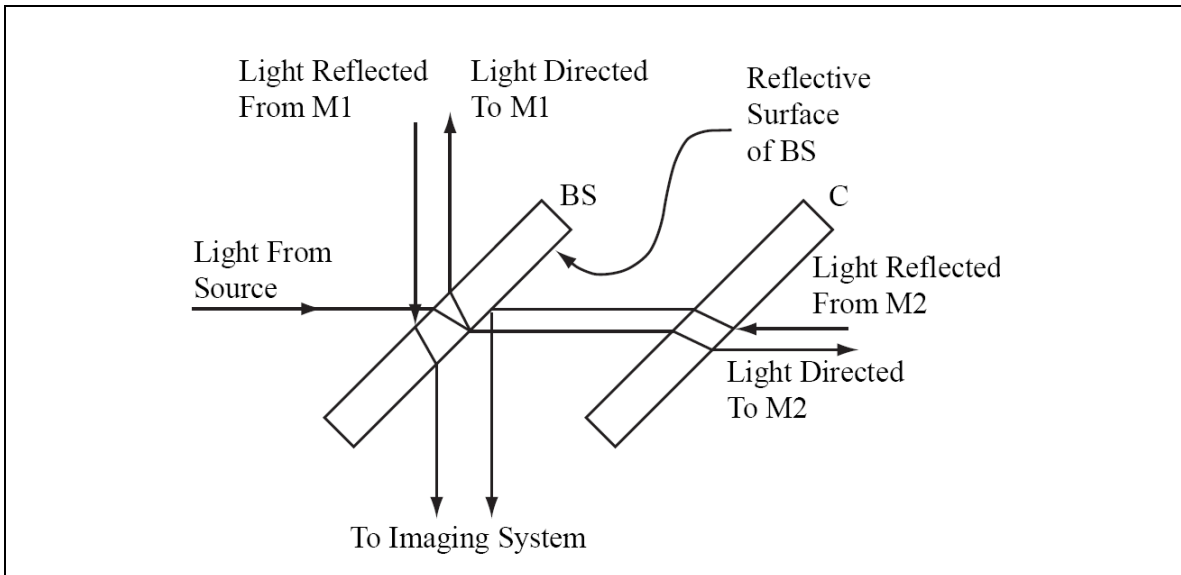


Figure 4.53. Michelson interferometer compensator plate. Compensator plate C is used to cancel dispersion from the glass of BS. With C in the system, each beam of the interferometer experiences three passes through the same thickness of glass.

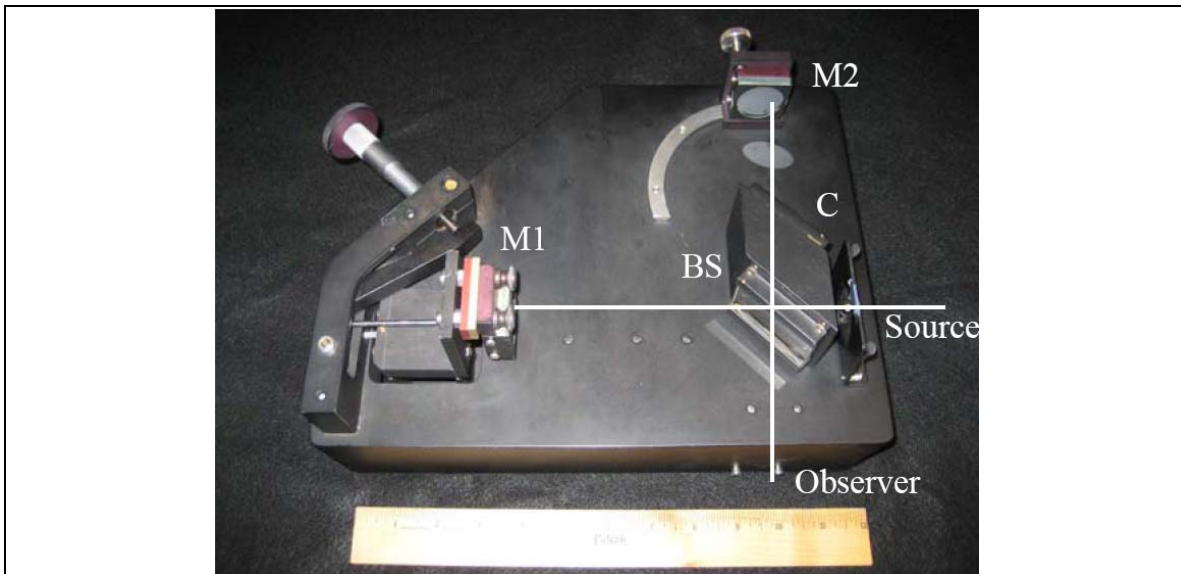


Figure 4.54. A student Michelson interferometer. In this case, the source is on the right side. The foreground ruler is 12 inches long.

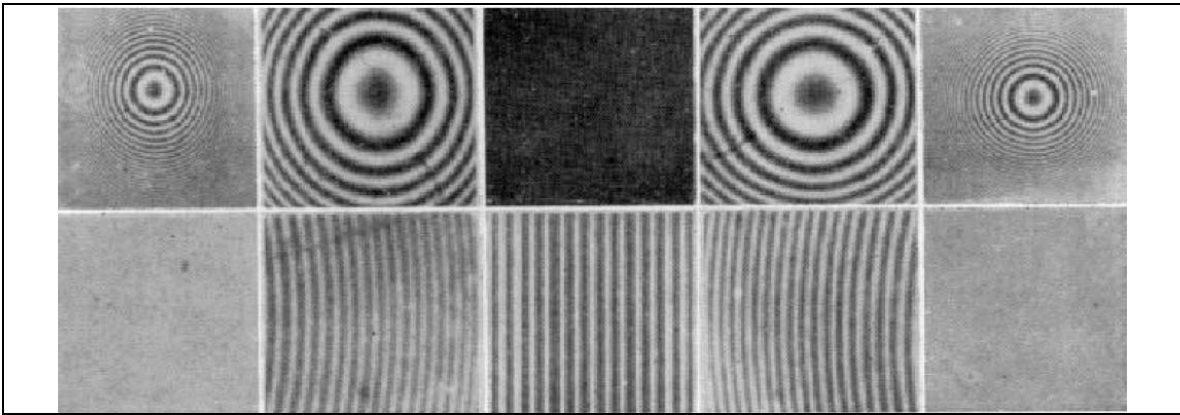


Figure 4.55. Summary of Michelson interferometer localization. Zero separation of the mirrors is in the center of each row. OPD increases positively to the right and negatively to the left away from the center. The upper row contains fringes of equal inclination (Haidinger's fringes). The bottom row contains fringes of equal thickness. [F.A. Jenkins and H. E. White, Fundamentals of Optics, 4<sup>th</sup> Ed., McGraw-Hill, Inc., New York, p. 274, (1976)]